ON THE ANTICLASTIC CURVATURE IN FREE EDGES AND THE CORNER TRANSVERSE SHEAR IN SOFT SIMPLY-SUPPORTED EDGES IN ANISOTROPIC RECTANGULAR THICK PLATES

Tales de Vargas Lisbôa

Rogério José Marczak

taleslisboa@daad-alumni.de

rato@mecanica.ufrgs.br

Department of Mechanical Engineering - Federal University of Rio Grande do Sul

Rua Sarmento Leite, 90050-170, Porto Alegre, Rio Grande do Sul, Brazil

Abstract. *The paper's objective is to revisit two phenomena of plate bending: the anticlastic curvature and the corner transverse shear and its relation to the reaction forces that can be observed in plates evaluated by the Kirchhoff Plate Theory. The anticlastic curvature is a phenomenon which occurs only in plates with two opposite free edges. The name is taken due to the opposite direction between the principal normal of the deformed plate, resulting in bending moments acting in opposite directions. It is shown that this response is dependent on the stiffness' ratio of the anisotropic material, affecting the size in which the anticlastic curvature can be observed. Another effect that can be noted in the plates evaluated by the classical plate theory is the reaction forces in non-smooth boundary regions, in simply- supported edges. Such phenomenon is generated by the twisting moment "jump", due to the abrupt geometric change. Given the kinematic hypothesis which bonds the transverse shear and the plate's rotation, the simply-supported boundary condition in Classical Plate Theory is translated to the soft simply-supported in Mindlin plate theory. These reaction forces are observable in Mindlin's theory as the transverse shear in a region close to the corner. By tending the thickness to zero, the region of transverse shear responsible to generate the reaction changes in format and gets close to a punctual force. The phenomena are presented and discussed.*

Keywords: *Anticlastic curvature, Corner transverse shear, anisotropic thick plates, thick plates in bending*

CILAMCE 2017
Proceedings of the XXXVIII Iberian Latin-American Congress on Computational Methods in Engineering
P.O. Faria, R.H. Lopez, L.F.F. Miguel, W.J.S. Gomes, M. Noronha (Editors), ABMEC, Florianpolis, SC, Brazil,
November 5-8, 2017

INTRODUCTION

In order to study the anticlastic curvature and the transverse shear at boundary non-smooth regions in anisotropic thick plates, the Mindlin plate theory (Mindlin, 1951; Reddy, 2007) is used. The *pb-2* Rayleigh-Ritz method (RRM) (Bhat, 1985; Liew & Wang, 1993) is employed to obtain the problem's equilibrium path in a semi-analytic fashion. Revisiting these contents – anticlastic curvature and the transverse shear at non-smooth regions – is considered relevant due to the little discussion with respect to their characteristics in anisotropic plates.

The Mindlin's theory (Mindlin, 1951) is a well-known first-order shear deformable theory (FSDT). Differently from the Kirchhoff Plate Theory (or zero-order shear deformable theory (ZSDT) (Reddy, 2007)), the plate's rotation is considered a new degree-of-freedom, varying linearly with the plate's thickness. As such, the transverse shear is taken into account in the deformation, contrasting with ZSDT. Given the discordance between the theoretical shear stress and the one obtained by Mindlin's theory, the transverse shear stress is weighted by a correction factor (Reddy, 2007; Jemielita, 2002). There are also other theories that consider the transverse shear strain in orders higher than the FSDT, known as high-order shear deformation theory(ies) (HSDT) (Reddy, 2007). They avoid the requirement of shear correction factors as they develop the transverse shear in the parabolic form. Nevertheless, boundary conditions lack physical explanation and should be cautiously analysed (Hanna & Leissa, 1994; Lo, Christensen, & Wu, 1977). In the FSDT, they have physical meaning and do not have to be condensed as the transverse shear and twisting moment as in Kirchhoff's theory.

The stress-strain relationship is given by the generalized Hooke's law. In FSDT, the constitutive tensor is reduced given a hypothesis on the stress field (Reddy, 2007; Alternbach, 1998). Depending on the atomic arrangement (crystalline symmetries) or the macroscopic behaviour (texture symmetries) (Cowin & Mehrabadi, 1995), the material behaviour may be categorise with respect to symmetries, which are defined essentially by the number and position of symmetric planes (Chadwick, Vianello, & Cowin, 2001; T. C. T. Ting, 2003). In three-dimensional elasticity, there exists eight different symmetries whereas in FSDT a triclinic material is not achievable, due to the constitutive symmetry plane parallel to the plate's mid-surface (Alternbach, 1998), resulting in seven different symmetries.

The *pb-2* Rayleigh-Ritz Method (RRM) (Bhat, 1985; Liew & Wang, 1993) is a modification of the original RRM and has been successfully applied to describe plate's mechanical behaviour. The *pb-2* modification eases the imposition of the problem's boundary conditions. The method has applied the method to obtain general thin plate's behaviour (Liew & Wang, 1993), response of plates with arbitrary shapes (Liew, 1992) and the transverse vibration of thick plates (Liew, Xiang, & Kitipornchai, 1993). It is clear the requirement of using the RRM variation in this paper: both effects herein studied are deeply dependent on the boundary conditions type and set. Moreover, one may obtain a semi-analytical global response using this method.

In further considering differences to the boundary conditions types and plates theories, it is well-known that both ZSDT and FSDT have three types of boundary conditions: clamped, simply-supported and free. In thick plates, each type of boundary condition has a hard and soft variation: they regard the imposition on the rotation (hard) or the twisting moment (soft) at the boundary (Haggblad & Bathe, 1990). Due to the aforementioned bond between the transverse displacement and the plate's rotations in the CPT, only soft boundary conditions are possible in this theory.

One interesting response that arises from these differences is the behaviour of the transverse shear close to non-smooth boundaries: the concentrated force (in the loading direction) appears at these position in CPT (Reddy, 2007). This force is responsible for a "jump" in the twisting moment at these regions. A physical explanation for such behaviour is the "corner-lifting". In thick plates, the same physical phenomena is observed. However, instead of a concentrated force, the transverse shear acts as a continuous function, changing its signal close to the aforementioned regions in soft simply-supported edges whereas in its hard counterpart, it tends zero. At the authors' best knowledge, little informations is found regarding anisotropy and shape/magnitude of the transverse shear at these regions. Investigations on different boundary conditions are also carried out so as to evaluate any relevant behaviour.

The anticlastic curvature is another interesting effect that occurs in plates with, at least, two free opposite edges. The two main curvatures, major and minor, have opposite directions and they magnitude can be related through the Poisson ratio, in isotropic materials (Hyer & Bhavani, 1984). The theme is revisited in order to analyse the effect with the different boundary conditions as well as different materials and principal directions. Cases of two and three sequential free edges are also analysed.

This report is organized as follows. In section two the governing equation of anisotropic moderately thick plates are presented. In section three the *pb-2* RRM is described and applied to the thick plates governing equations. In section four, the solutions obtained and both analysis are outlined. The paper is concluded in section five. This paper is part of a major research in a new procedure in evaluating anisotropic responses by enhancing isotropic ones (Lisbôa, Geiger, & Marczak, 2017; Lisbôa & Marczak, 2017).

Both matrix and index notation are used. Bold-face lower and upper-case denote 1st and 2nd order tensors, respectively, whereas non-indexed symbols describe scalars. All vectors are defined as column-vector. In index notation, lower and upper-case indices ranges from 1 to 3 and 1 to N, respectively, while Greek indices varies from 1 to 2.

MODELLING

Consider an anisotropic a homogeneous plate with uniform thickness in a rectangular domain as represented in Fig. 1. The displacement field is written as

$$\begin{aligned} U_1(x_1, x_2, x_3) &\doteq -x_3\theta_1(x_1, x_2) \ , \\ U_2(x_1, x_2, x_3) &\doteq -x_3\theta_2(x_1, x_2) \ , \\ U_3(x_1, x_2) &\doteq u_3(x_1, x_2) \ , \end{aligned} \tag{1}$$

where U_k denote the orthogonal displacement components, θ_α describe the rotation in relation of the mid-surface in the α direction and u_3 corresponds to the transverse displacement. As depicted in Fig. 1, x_k represent the Cartesian coordinates, Ω and Λ denote the plate's volume and mid-surface, respectively. The vectors $\mathbf{n}$ and $\mathbf{t}$, shown in a transverse cut, are the outwards normal and the tangent unit vectors of $\partial\Lambda$, respectively. In-plane degrees-of-freedom are not expressed in the Eq. (1) due to the decoupling between the membrane and bending effects, as expected in a homogeneous plate in linear bending.

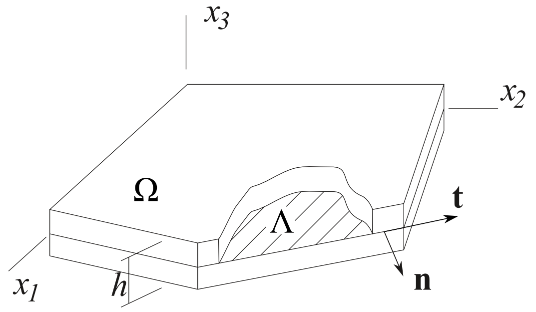

Figure 1: Plate's Domain

The strain-displacement relation is written as

$$\boldsymbol{\epsilon} = \mathbf{H}\boldsymbol{\partial}\mathbf{d}\,,$$

where

$$\boldsymbol{\epsilon} = \begin{Bmatrix} \epsilon_{11} \\ \epsilon_{22} \\ \epsilon_{23} \\ \epsilon_{13} \\ \epsilon_{12} \end{Bmatrix}, \quad \mathbf{H} = \begin{bmatrix} 0 & 0 & -x_3 & 0 & 0 \\ 0 & 0 & 0 & -x_3 & 0 \\ 1 & 0 & 0 & 0 & 0 \\ 0 & 1 & 0 & 0 & 0 \\ 0 & 0 & 0 & 0 & -x_3 \end{bmatrix}, \quad \boldsymbol{\partial} = \begin{bmatrix} \dfrac{\partial}{\partial x_2} & 0 & -1 \\ \dfrac{\partial}{\partial x_1} & -1 & 0 \\ 0 & \dfrac{\partial}{\partial x_1} & 0 \\ 0 & 0 & \dfrac{\partial}{\partial x_2} \\ 0 & \dfrac{\partial}{\partial x_2} & \dfrac{\partial}{\partial x_2} \end{bmatrix},$$

and the plate's degrees-of-freedom are

$$\mathbf{d} = \begin{Bmatrix} u_3 & \theta_1 & \theta_2 \end{Bmatrix}^{\mathrm{T}}.$$

As a consequence of the plate's thickness remaining constant ($\epsilon_{33} = 0$) through the equilibrium path, the constitutive relationship is modified accordingly, resulting in (Reddy, 2007)

$$\boldsymbol{\sigma} = \mathbf{Q}\boldsymbol{\epsilon}\,, \qquad \mathbf{Q} = \mathbf{R}^{-1}\hat{\mathbf{C}}\mathbf{R}\,,$$

where $\mathbf{Q}$, $\mathbf{R}$ and $\hat{\mathbf{C}}$ are the transformed constitutive tensor, the transformation matrix and the reduced constitutive tensor, respectively. $\mathbf{R}$ relates the material and the plate's coordinate systems. In its principal directions, $\hat{\mathbf{C}}$ is given

$$\hat{\mathbf{C}} = \begin{bmatrix} \hat{C}_{11} & \hat{C}_{12} & 0 & 0 & \hat{C}_{16} \\ & \hat{C}_{22} & 0 & 0 & \hat{C}_{26} \\ & & \kappa_{11}\hat{C}_{44} & \kappa_{12}\hat{C}_{45} & 0 \\ & & & \kappa_{22}\hat{C}_{55} & 0 \\ sym & & & & \hat{C}_{66} \end{bmatrix}, \tag{2}$$

where

$$\hat{\mathbf{C}} \doteq C_{IJ}^{\mathrm{RED}} = C_{IJ} - \frac{1}{C_{33}} C_{I3} C_{3J} \, ,$$

with $\mathbf{C}$ and $\mathbf{C}^{\mathrm{RED}}$ denoting the 6×6 anisotropic constitutive tensor and the 6×6 reduced anisotropic constitutive tensor with the 3rd line/column populated with zeros, respectively. $\hat{\mathbf{C}}$ is then assembled by excluding the 3rd line/column from $\mathbf{C}^{\mathrm{RED}}$.

The shear correction factors are set as $\kappa_{\alpha\beta} = \frac{5}{6}$ (Reddy, 2007; Jemielita, 2002). The constitutive tensor in Eq. (2) represents a monoclinic symmetry (9 independent constants). As explained by Altenbach (Alternbach, 1998), given the plate's geometry, the material has a plane of symmetry parallel to the mid-surface, characterising monoclinic symmetry or any lower, with respect to the complexity of the symmetry.

The bending (M_{11}, M_{22}) and twisting (M_{12}) moments as well as the transverse shear stresses (S_{13}, S_{23}) are written as (Reddy, 2007, 2004)

$$\mathbf{M} = \mathbf{D}\boldsymbol{\varepsilon}^{\mathrm{B}} \, , \qquad \mathbf{D} = \frac{h^3}{12}\hat{\mathbf{C}}^{\mathrm{B}} \, , \qquad \boldsymbol{\varepsilon}^{\mathrm{B}} = \begin{Bmatrix} \theta_{1,1} & \theta_{2,2} & \theta_{1,2} + \theta_{2,1} \end{Bmatrix}^{\mathrm{T}} \, ,$$
$$\mathbf{S} = \mathbf{A}\boldsymbol{\varepsilon}^{\mathrm{S}} \, , \qquad \mathbf{A} = h\hat{\mathbf{C}}^{\mathrm{S}} \, , \qquad \boldsymbol{\varepsilon}^{\mathrm{S}} = \begin{Bmatrix} u_{3,2} - \theta_2 & u_{3,1} - \theta_1 \end{Bmatrix}^{\mathrm{T}} \, ,$$

where $\mathbf{D}$ and $\mathbf{A}$ are the bending and extensional stiffness matrices, respectively, and

$$\hat{\mathbf{C}}^{\mathrm{B}} = \begin{bmatrix} \hat{C}_{11} & \hat{C}_{12} & \hat{C}_{16} \\ & \hat{C}_{22} & \hat{C}_{26} \\ \mathrm{sym.} & & \hat{C}_{66} \end{bmatrix} , \qquad \hat{\mathbf{C}}^{\mathrm{S}} = \begin{bmatrix} \kappa_{11}\hat{C}_{44} & \kappa_{12}\hat{C}_{45} \\ \mathrm{sym.} & \kappa_{22}\hat{C}_{55} \end{bmatrix} .$$

with

$$\mathbf{M} = \begin{Bmatrix} M_{11} & M_{22} & M_{12} \end{Bmatrix}^{\mathrm{T}} , \qquad \mathbf{S} = \begin{Bmatrix} S_{23} & S_{13} \end{Bmatrix}^{\mathrm{T}} .$$

and $\boldsymbol{\varepsilon}^{\mathrm{B}}$ describing the strain field due to the bending whereas $\boldsymbol{\varepsilon}^{\mathrm{S}}$ presents it regarding the transverse shear evaluation.

The equilibrium in terms of the resultant stresses are then defined as (Reddy, 2007)

$$\begin{aligned} M_{\alpha\beta,\beta} - S_{3\alpha} &= 0 \, , \\ S_{\alpha 3,\alpha} + q_3 &= 0 \, , \end{aligned} \tag{3}$$

where q_3 refers to the transverse loading. Equation (3) can be also written in terms of the transverse displacement and rotations using elementary stress-displacements relations (Reddy, 2007). Moreover, it is written in absence of distributed moments as only transverse loading is considered in this report.

The boundary conditions for a thick plate problem (Fig. 1)

$$\begin{array}{llll}
\bullet \ \text{Clamped Edge :} & \overline{u}_3 = 0 \text{ on } \partial\Lambda_u\,, & \overline{\theta}_{\mathbf{n}} = 0 \text{ on } \partial\Lambda_u\,, & \overline{\theta}_{\mathbf{t}} = 0 \text{ on } \partial\Lambda_u\,, \\
\bullet \ \text{Hard Simply-Suported Edge :} & \overline{u}_3 = 0 \text{ on } \partial\Lambda_u\,, & \overline{\theta}_{\mathbf{t}} = 0 \text{ on } \partial\Lambda_u\,, & \overline{M}_{\mathbf{nn}} = 0 \text{ on } \partial\Lambda_n\,, \\
\bullet \ \text{Soft Simply-Suported Edge :} & \overline{u}_3 = 0 \text{ on } \partial\Lambda_u\,, & \overline{M}_{\mathbf{nn}} = 0 \text{ on } \partial\Lambda_n\,, & \overline{M}_{\mathbf{nt}} = 0 \text{ on } \partial\Lambda_n\,, \\
\bullet \ \text{Free Edge :} & \overline{S}_{\mathbf{n}3} = 0 \text{ on } \partial\Lambda_n & \overline{M}_{\mathbf{nn}} = 0 \text{ on } \partial\Lambda_n\,, & \overline{M}_{\mathbf{nt}} = 0 \text{ on } \partial\Lambda_n\,,
\end{array} \tag{4}$$

where $\partial\Lambda_e \cup \partial\Lambda_n = \partial\Lambda$, $\partial\Lambda_e \cap \partial\Lambda_n = \varnothing$, $\partial\Lambda_e$ and $\partial\Lambda_n$ are the boundary parts in which the essential and natural boundary conditions are imposed, respectively.

It is worth to note that boundary layer effects are more significant in soft simply-supported boundary conditions than in its hard counterpart (Haggblad & Bathe, 1990). The clamped edge boundary condition has also the possibility of having hard and soft conditions, though the soft one ($\overline{\theta}_{\mathbf{t}} \neq 0; \quad \overline{M}_{\mathbf{nt}} = 0$) is not considered in the studies due to the fact that the boundary layer is the weakest among all the thick plates boundary conditions types and variations (Haggblad & Bathe, 1990).

In order to apply the RRM, the plate's strain energy, W_{int}, is evaluated as

$$W_{\text{int}} = \frac{1}{2}\int_{\Omega} \boldsymbol{\sigma}^{\text{T}}\boldsymbol{\epsilon}\;\mathrm{d}\Omega = \frac{1}{2}\int_{\Omega} \mathbf{d}^{\text{T}}\boldsymbol{\partial}^{\text{T}}\mathbf{H}^{\text{T}}\hat{\mathbf{C}}\mathbf{H}\boldsymbol{\partial}\mathbf{d}\;\mathrm{d}\Omega = \frac{1}{2}\int_{\Lambda} \mathbf{d}^{\text{T}}\boldsymbol{\partial}^{\text{T}}\mathbf{T}\boldsymbol{\partial}\mathbf{d}\;\mathrm{d}\Lambda\,,$$

where the matrix $\mathbf{T}$ is characterised by

$$\mathbf{T} = \int_{-h/2}^{h/2} \mathbf{H}^{\text{T}}\hat{\mathbf{C}}\mathbf{H}\;\mathrm{d}x_3\,,$$

Also the external potential, W_{ext}, is determined as

$$W_{\text{ext}} = -\int_{\Lambda} \mathbf{q}^{\text{T}}\mathbf{d}\;d\Lambda\,,$$

where

$$\mathbf{q} = \begin{Bmatrix} q_3 & 0 & 0 \end{Bmatrix}^{\text{T}}$$

and $\mathbf{q}$ corresponds to the loading vector.

THE *PB-2* RAYLEIGH-RITZ METHOD

The *pb-2* Rayleigh-Ritz Method (Liew & Wang, 1993; Kitipornchai, Xiang, Liew, & Lim, 1994; Liew, 1992) is a modification of the original method where the boundary conditions are imposed by monomials (Bhat's beam functions) multiplying the solution approximation (Bhat, 1985).

In the present case, the degrees-of-freedom are interpolated by

$$\mathbf{d} = \boldsymbol{\Phi}\boldsymbol{\lambda},$$

			γ_k	
		$g^{(1)}$	$g^{(2)}$	$g^{(3)}$
• Clamped	(C)	1	1	1
• Hard Simply-Supported	(H)	1	1	0
• Soft Simply-Supported	(S)	1	0	0
• Free	(F)	0	0	0

Table 1: γ_k values to the corresponding boundary conditions

where

$$\mathbf{\Phi} = \begin{bmatrix} \boldsymbol{\phi}^{(1)^{\mathrm{T}}} & \mathbf{0} & \mathbf{0} \\ \mathbf{0} & \boldsymbol{\phi}^{(2)^{\mathrm{T}}} & \mathbf{0} \\ \mathbf{0} & \mathbf{0} & \boldsymbol{\phi}^{(3)^{\mathrm{T}}} \end{bmatrix}_{3\times 3n} \quad , \boldsymbol{\lambda} = \begin{Bmatrix} \mathbf{c}^{(1)} \\ \mathbf{c}^{(2)} \\ \mathbf{c}^{(3)} \end{Bmatrix}_{3n} ,$$

and

$$\mathbf{c}^{(i)^{\mathrm{T}}} = \begin{Bmatrix} c_1^{(i)} & c_2^{(i)} & c_3^{(i)} & \dots & c_n^{(i)} \end{Bmatrix}_n ,$$

where $\boldsymbol{\phi}^{(i)}$ denote kinematic admissible functions, the vector $\boldsymbol{\lambda}$ groups the constants of the linear combination, defined by $\mathbf{c}^{(i)}$, i is the ith degrees-of-freedom and n the number of weighting constants for each degree-of-freedom, which is closely related to the approximation's enrichment (Liew, 1992). The boundary conditions are imposed by the following product of monomials, $g^{(\mathrm{i})}$,

$$g^{(\mathrm{i})}(x_1, x_2) = \prod_{k=1}^{4} [\Theta_k (x_1, x_2)]^{\gamma_k} ,$$

in which γ_k is a exponent related to the boundary condition's type and Θ_k are the line equations of the boundary. In the case of $[0, a] \times [0, b]$ rectangular plate, for instance, the boundary is defined by

$$\Theta_1 = x_2, \qquad \Theta_2 = x_1 - a, \qquad \Theta_3 = x_2 - b, \qquad \Theta_4 = x_1.$$

The final interpolation functions are then given by

$$\boldsymbol{\phi}^{(\mathrm{i})}(x_1, x_2) = g^{(\mathrm{i})}(x_1, x_2)\, \boldsymbol{\omega}(x_1, x_2) , \tag{5}$$

where $\boldsymbol{\omega}$ is a vector containing a trial basis (no longer with the requirement of being kinematically admissible). The construction of $\boldsymbol{\phi}^{(i)}$ is a dyadic product between the monomial power sequence in x_1 and x_2 (Liew, 1992), when polynomials are used to approximate the solution space.

For FSDT plates, γ_k can be either 0 (null) or 1 (one) for the usual boundary conditions as Tab.1. The letters C, H, S and F from now on indicate the boundary condition type. In hard simply-supported, the restricted rotation concerns the normal direction, consequently, the values of $g^{(2)}$ and $g^{(3)}$ can be exchanged.

In order to simplify the numerical integration, the plate domain is mapped to a normalised space $s_1 \times s_2 = [-1,1] \times [-1,1]$, and the strain energy and the external potential are both written as a function of $\boldsymbol{\lambda}$ as

$$W_{\text{int}} = \frac{1}{2}\boldsymbol{\lambda}^{\mathrm{T}} \int_{-1}^{1}\int_{-1}^{1} \boldsymbol{\Phi}^{\mathrm{T}}\boldsymbol{\partial}^{\mathrm{T}}\mathbf{T}\boldsymbol{\partial}\boldsymbol{\Phi}\,|\mathbf{J}|\,\mathrm{d}s_1\mathrm{d}s_2\,\boldsymbol{\lambda} = \frac{1}{2}\boldsymbol{\lambda}^{\mathrm{T}} \int_{-1}^{1}\int_{-1}^{1} \mathbf{B}^{\mathrm{T}}\mathbf{T}\mathbf{B}\,|\mathbf{J}|\,\mathrm{d}s_1\mathrm{d}s_2\,\boldsymbol{\lambda},$$

$$W_{\text{ext}} = -\int_{-1}^{1}\int_{-1}^{1} \mathbf{q}^{\mathrm{T}}\boldsymbol{\Phi}\,|\mathbf{J}|\,\mathrm{d}s_1\mathrm{d}s_2\,\boldsymbol{\lambda}.$$

in which $|\mathbf{J}|$ corresponds to the Jacobian (between the original and normalised coordinates).

The first variation of total energy potential is obtained with

$$\frac{\partial W_{\text{int}}}{\partial \boldsymbol{\lambda}} = \int_{-1}^{1}\int_{-1}^{1} \mathbf{B}^{\mathrm{T}}\mathbf{T}\mathbf{B}\,|\mathbf{J}|\,\mathrm{d}s_1\mathrm{d}s_2\,\boldsymbol{\lambda} = \mathbf{N}\boldsymbol{\lambda}$$

$$\frac{\partial \mathrm{W}_{\text{ext}}}{\partial \boldsymbol{\lambda}} = -\int_{-1}^{1}\int_{-1}^{1} \boldsymbol{\Phi}^{\mathrm{T}}\mathbf{q}\,|\mathbf{J}|\,\mathrm{d}s_1\mathrm{d}s_2 = -\mathbf{v}$$

resulting in the equilibrium equation

$$\mathbf{N}\boldsymbol{\lambda} = \mathbf{v}$$

RESULTS

A numeric routine is developed so as to determine solutions for both anticlastic curvature and transverse shear close to non-smooth regions. Firstly, the RRM convergence is shown. Then the anticlastic curvature is presented for four cases: two examples with opposite edges, one simulating a cantilever plate and the last with only one free edge. After, the transverse shear at corners is studied for three boundary conditions sets containing soft simply-supported edges, aiming the assessment of possible modifications on the transverse shear with respect to them at regions close to the corners. All responses are compared with numeric results obtained by the Finite Element Method using a commercial software (Ansys ® Inc., 2017).

The material properties in all numeric analysis is set as (Lisbôa et al., 2017; H.-T. Ting & Kim, 2012)

$$E_{11} = \alpha E_{22}, \qquad G_{12} = 0.6E_{22}, \qquad G_{13} = 0.5E_{22}, \qquad G_{23} = 0.6E_{22}, \qquad \nu_{12} = 0.25,$$

which belongs to an orthorhombic symmetry. The constitutive properties are then written as

$$\hat{C}_{11} = \frac{E_{11}}{1-\nu_{12}\nu_{21}}, \qquad \hat{C}_{22} = \frac{E_{22}}{1-\nu_{12}\nu_{21}}, \qquad \hat{C}_{12} = \frac{E_{22}\nu_{21}}{1-\nu_{12}\nu_{21}},$$
$$\hat{C}_{44} = G_{23}, \qquad \hat{C}_{55} = G_{13}, \qquad \hat{C}_{66} = G_{12},$$

p	$\hat{w}^C$	M_{11}^C	M_{22}^C	$\hat{S}_{23}^N$	$\hat{S}_{13}^E$
5	0.911089262	0.066065184	0.000733963	-0.16617463	-0.174469298
7	0.928631204	0.066360942	0.001643128	-0.138017881	-0.196620918
9	0.928000988	0.066371008	0.001560212	-0.131586019	-0.192754324
11	0.928068452	0.066437044	0.001584565	-0.132669916	-0.191826266
13	0.928035208	0.066396291	0.001568784	-0.13358482	-0.192286426
15	0.928029044	0.06642468	0.001575886	-0.133702089	-0.192609325
17	0.928037631	0.066404969	0.001571562	-0.133544144	-0.192209221
19	0.928030625	0.066418187	0.001574541	-0.133439515	-0.192382608
$\star$	0.927989	0.66105922	0.01562882	-0.132335825	-0.191102555

$\star$ (Ansys ® Inc., 2017)

Table 2: Convergence for rectangular HHCC plates with $\alpha = 10$ and $a/h = 10$ under uniform loading

and $\nu_{12}E_{22} = \nu_{21}E_{11}$.

In order to present the obtained results some variables are made non-dimensional as follow (H.-T. Ting & Kim, 2012)

$$\hat{w}^{\text{pos}} = \frac{100u_3(x_1^{\text{pos}}, x_2^{\text{pos}})E_2h^3}{q_3a^4}, \qquad \hat{M}_{\alpha\beta}^{\text{pos}} = \frac{M_{\alpha\beta}(x_1^{\text{pos}}, x_2^{\text{pos}})}{q_3a^2}, \qquad \hat{S}_{\alpha 3} = \frac{S_{\alpha 3}(x_1^{\text{pos}}, x_2^{\text{pos}})}{2q_3a},$$

and

$$\hat{w}_{ref}^{\text{pos}} = \frac{\hat{w}^{\text{pos}}}{\hat{w}_{ref}^{\,c}}, \qquad \hat{w}^{\text{conv}} = \frac{\hat{w}_{n_{int}}}{\hat{w}_{ref}^{\,c}}, \qquad \hat{M}_{ref}^{(\alpha\beta)} = \frac{\hat{M}_{\alpha\beta}}{\hat{M}_{ref}^{\,c}}, \qquad \hat{Q}_{ref}^{(\alpha)} = \frac{\hat{S}_{\alpha 3}}{\hat{S}_{ref}^{\,c}}, \tag{6}$$

noticing that $(\hat{\cdot})$ and $(\cdot)_{ref}$ denote non-dimensional variables and reference (converged) values, respectively. pos corresponds to the assessed position as $\text{pos} = \{\text{C}, \text{N}, \text{S}, \text{E}, \text{W}, \text{NE}\}$ and are related to the cardinal directions taken from (C)entre. $\hat{w}^{\text{conv}}$ presents the ratio between the iteration centre displacement and the converged one. $\hat{Q}_{ref}^{(\alpha)}$ and $\hat{M}_{ref}^{(\alpha\beta)}$ are assessed in the same position for all analysis: $\hat{Q}_{ref}^{(1)}$ in $\text{pos} = \text{E}$, $\hat{Q}_{ref}^{(2)}$ in $\text{pos} = \text{N}$ and $\hat{M}_{ref}^{(\alpha\beta)}$ in $\text{pos} = \text{C}$.

So as to define a solution reference, numeric results are obtained by FEM using a 8-node shell element (Ansys ® Inc., 2017) based on Mindlin's plate theory. A mesh of 200 elements per metre is considered. Such mesh as necessary given FEM's low rate of convergence for transverse shear stress. Moreover, the boundary condition sets are described by four upper-case letters, regarding Tab. 1, starting from the south edge and turning anticlockwise.

Convergence

Table 2 shows the RRM convergence for transverse displacement, bending moments and transverse shear in rectangular HHCC plates with $\alpha = 10$ and $a/h = 10$. p denotes the polynomial degree of $\boldsymbol{\omega}$ (eq. (5)). As one can notice, only odd values of p are presented in the aforementioned tables. In this regard, even values develop results with small gain concerning convergence criteria with respect to those obtained with a p immediately before.

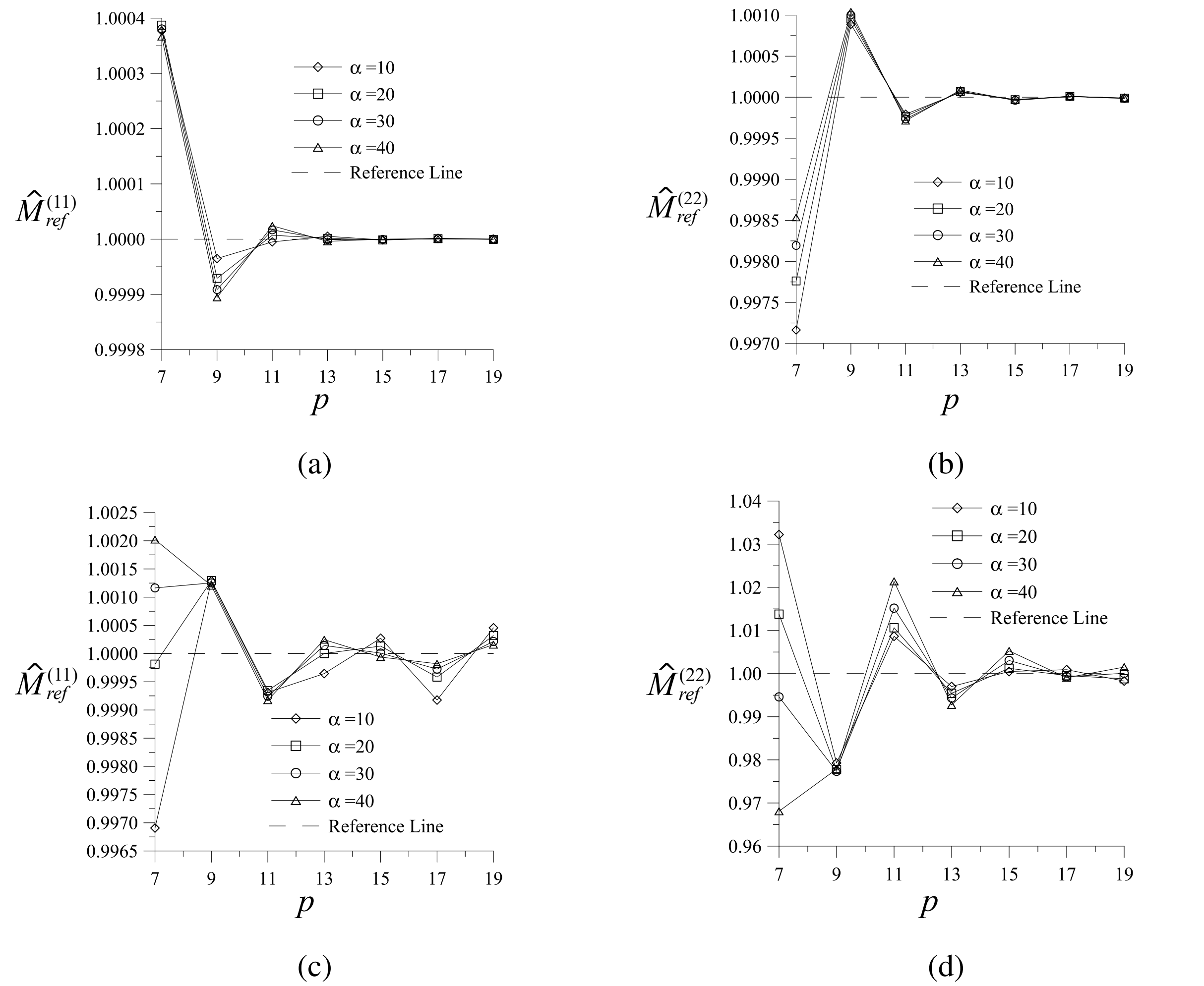

Figure 2: Bending moments convergence of square FHFH with $a/h = 5$: (a) M_{11} and (b) M_{22} in the plate's centre. Bending moments convergence of square CFFC with $a/h = 5$: (c) M_{11} and (d) M_{22} in the plate's centre.

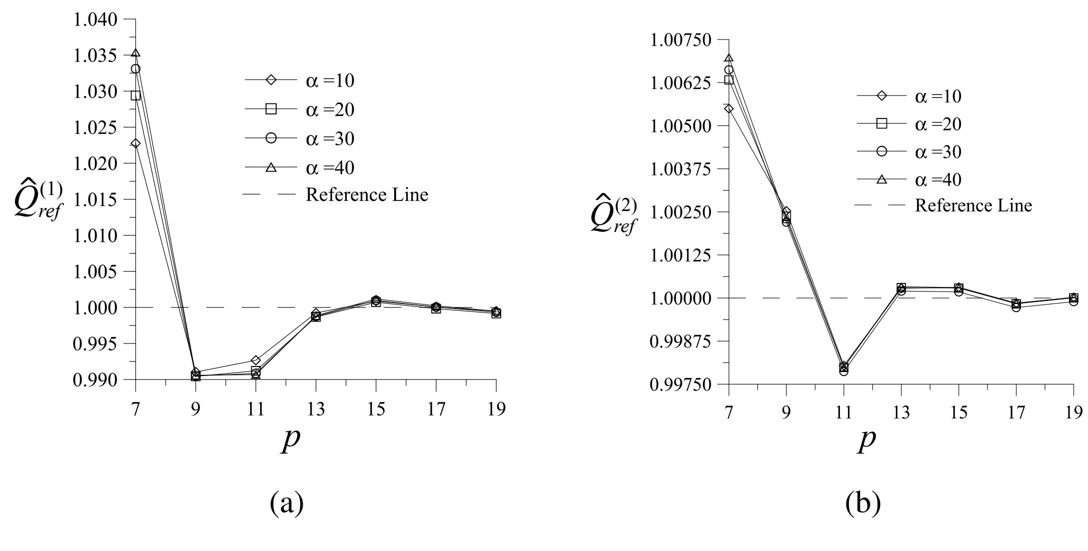

Figure 3: Transverse shear convergence for rectangular HHHH plates with $a/h = 5$: (a) S_{13} and (b) S_{23}.

The precision level of 4 digits of significance was achieved with $p = 13$, for transverse displacement. Small divergences are observable regarding the converged values and FEM ones in bending moments and in transverse shear. The maximum relative error was smaller than 1%. This corresponds to a small discrepancy at the third digit. Mostly, such high errors were found in transverse shear comparisons (for other boundary conditions than the presented in Tab. 2), being this an expected behaviour: given the relationship between the interpolated variables (displacements) and the transverse shear, the convergence rate might be (and it was) slower than the displacement and rotations.

Bending moments and transverse shear convergence are further analysed, as depicted in Figs. 2 and 3. The first present the convergence for two boundary conditions sets – FHFH and CFFC and they are among the worst with respect to this property. Moreover, material properties are also varied. The second figure concerns the convergence of the transverse shear in rectangular HHHH plates. In spite of being well-behaved in Fig. 3, the convergence of the transverse shear is severely jeopardised as a/h increases. Examples of it are presented next.

Results and Discussion

Anticlastic curvature

After presenting the convergence of RRM, the anticlastic curvature effect can be evaluated. Figure 4 presents the transverse displacement of (half of) free edge opposite to the clamped one in a CFFF plate. The displacement is normalised by the one at the free edge center. The anticlastic curvature can be viewed as a analogous response to the Saint-Venant beam displacement field of the transverse area. As one notes, independently of the a/h and α, the anticlastic curvature "shape" is the same. The effect magnitude is almost insensible to the variation of these parameters. Moreover, the effect's magnitude is relatively small: circa 1% of the maximum transverse displacement. The major curvature is this case is naturally pointed upwards.

Figures 5 and 6 depict the anticlastic curvature for CFCF and FCFC, normalised by the center transverse displacement and with respect to material properties and a/h ratios. It is worth to note that the major curvature is pointed downwards for both cases and the edge evaluated is different for each case. By both figures, one observes that only the magnitude is affected by α and a/h. As aforementioned, the anticlastic curvature is linked with the Poisson's ratio (Hyer & Bhavani, 1984). By the formula that correlates the major, ν_{12}, and minor, ν_{21}, Poisson's ratio (regarding the elastic modulus), as α increases, ν_{21} decreases. The major difference are a consequence of the boundary conditions and the direction of the larger elastic modulus. This can also be observed in Fig. 6 given the fact that ν_{12} is fixed.

Furthermore, a compelling phenomena is shown in Figures 6, magnified in thinner plates: the minor curvature close to the plate's centre has the same direction of the major one; next to the free edge, this direction changes. Even for $a/h = 10$ in FCFC plates (plate relatively thick), this behaviour can be observed. This happens given the fact that the smallest elastic modulus is in such direction and the larger is the difference between the modulus, the larger this effect is. The magnitude of the effect, with respect to the center transverse displacement varies from 0.5% to 4%.

The anticlastic curvature could not be noted, however, in the cases with two sequential free-edges. In Fig. 7, both free edges of a SFFS plate are verified, considering the same parameters

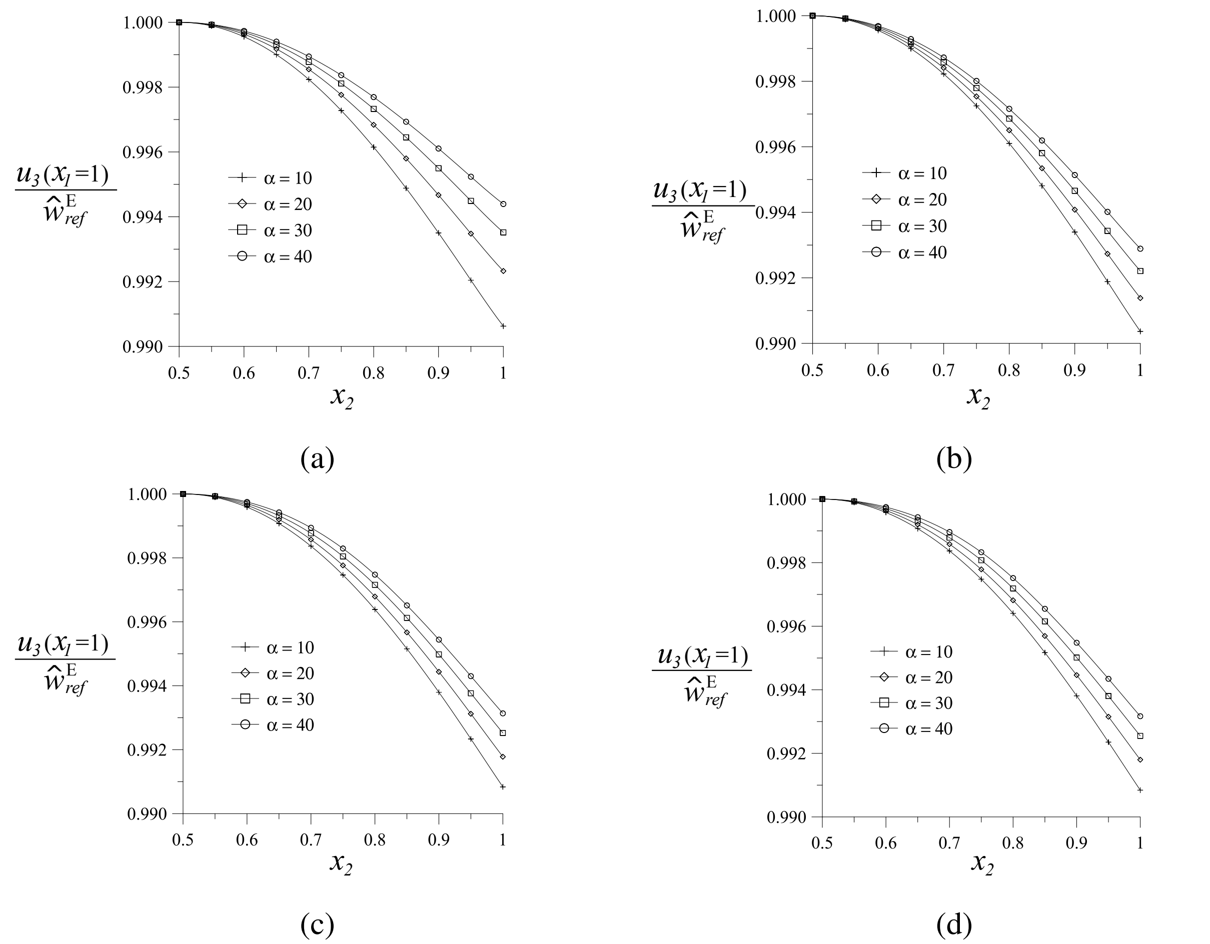

Figure 4: Anticlastic curvature in square FFFC plates: (a) $a/h = 5$**, (b)** $a/h = 10$**, (c)** $a/h = 50$ **and (d)** $a/h = 100$**.**

of the previous cases. Despite not concerning the evaluation herein proposed, the free edge displacement appears to be indifferent to both a/h and α.

Analogously, in spite of not being presented, plates with just one free edge will not present such characteristics. The direction of the curvature is mainly determined by the loading direction and the opposite boundary conditions, in rectangular plates. With the proposed loading direction (upwards), any configuration that excludes free edges in two opposite directions generates a negative curvature. A composition between a free and a non-free edge obtains a negative or null curvature (Figure 7).

Transverse shear at corners

It is well-known in CPT reactions at corners occur naturally in simply-supported edges. Such effect is related to the twisting moment, to the non-smoothness of the boundary and to the kinematic hypothesis that bonds the transverse displacement and rotations. Basically, there is a "jump" in the twisting moment in non-smooth boundary and this concentrated force is responsible for it.

The physical phenomena is also known as corner lifting and it can be observed if, for ex-

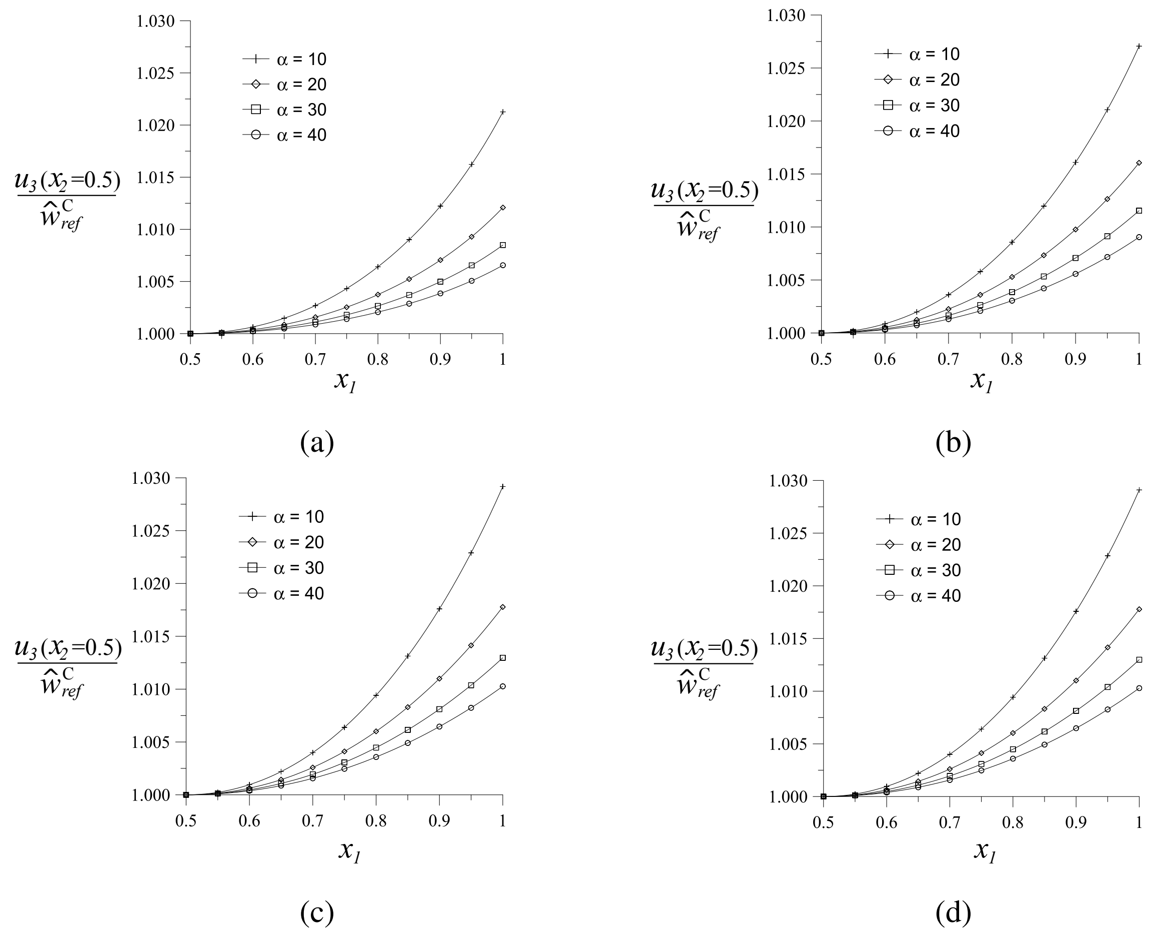

Figure 5: Anticlastic curvature in square CFCF plates: (a) $a/h = 5$**, (b)** $a/h = 10$**, (c)** $a/h = 50$ **and (d)** $a/h = 100$**.**

ample, a negative lateral force is applied to a variation of simply-supported boundary condition where the edges could not move downwards, only upwards. The regions close to the corners tend to move upwards. Due to the fact that simply-supported boundary condition restricts both movements (up- and downwards), in order to impose such restriction, this concentrated force appears.

One can observe this effect in FSDT likewise, in a continuous manner. Firstly, one notices that there are two types of simply-supported boundary conditions in FSDT: soft and hard and their difference concerns to the imposition over the tangential rotation or twisting moment (eq. (4)). The hard boundary conditions imposes a restriction on the tangential rotation on the edge, generating a non-null twisting moment, which is responsible for avoiding the corner to lift. Therefore, the transverse shear force is null in the corner. Nevertheless, in the soft boundary condition, there are no restriction over the plate's rotations on the edge, which results in a null twisting moment. Thus, the transverse shear in non-null and it is similar to the reaction force on corners, in the CPT.

An interesting behaviour is as the plate thickness is reduced, the region that the transverse shear is pointed to the same direction of the loading is also reduced. Its value at the corner,

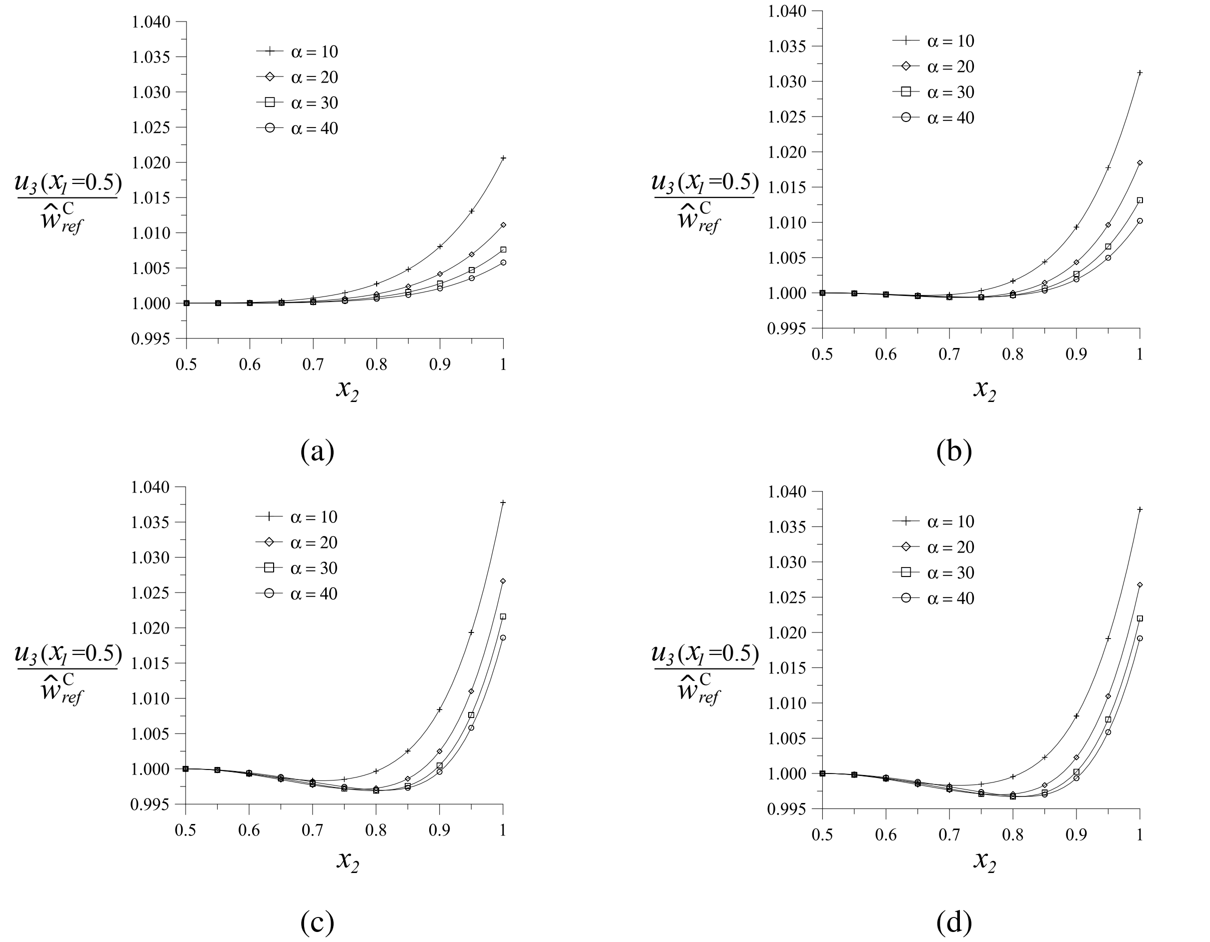

Figure 6: Anticlastic curvature in square FCFC plates: (a) $a/h = 5$**, (b)** $a/h = 10$**, (c)** $a/h = 50$ **and (d)** $a/h = 100$**.**

however, increases exponentially. This behaviour is also observed in ref. (Haggblad & Bathe, 1990), which is a clear correlation between ZSDT and FSDT: as h tends to zero, the response of a thick plate tends to the one of a thin plate, including naturally the concentrated force at corners. Given this “pathology” and the approximation procedure, the entire solution of transverse shear loses precision and requires more terms to avoid the oscillations.

Firstly, it is presented the differences between both boundary conditions (soft and hard) in Fig. 8 for both S_{13} and S_{23}. The edge is partially considered. In Fig. 8 (a), five values of a/h are depicted and they corroborate the analytical explanation. For three values of a/h, their value of S_{13} are out of the graph scale. One may also observe that for greater values of a/h, the transverse shear oscillates. Figure 8 (b) is used as a comparison: no oscillation nor pathological behaviour is observable.

Figure 9 shows then the variation between the transverse shear S_{13}/S_{23} and α. $1/4$ of the plate’s edge is evaluated. The transverse shear aforementioned behaviour of exponentially growing can be noted for thinner plates in all cases. Moreover, the differences with respect to a/h tend to diminish as the evaluation region gets closer to the edge’s center. The magnitude of the transverse shear at corners is greatly influenced by α whereas in the direction of the edge’s

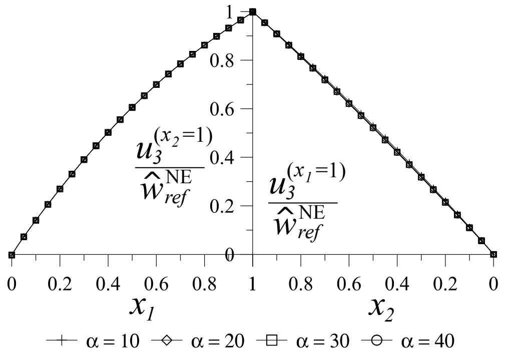

(a)

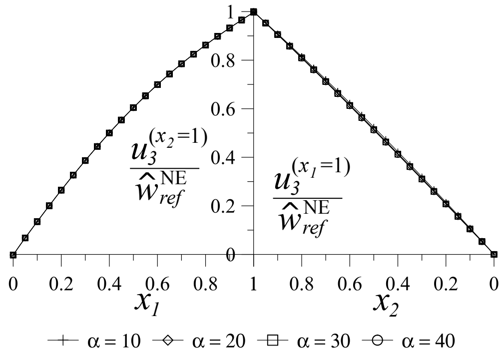

(b)

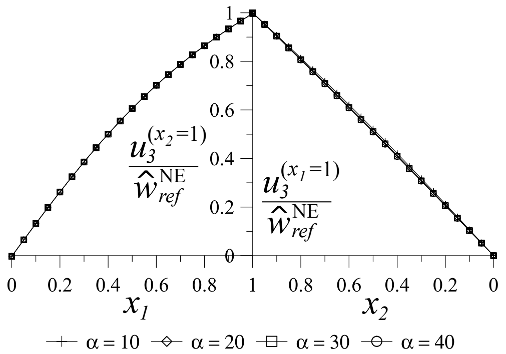

(c)

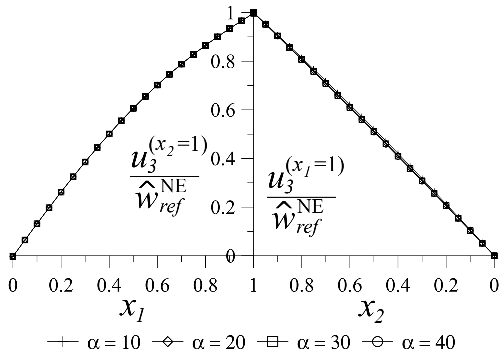

(d)

Figure 7: Transverse displacement at free edges in square SFFS plates: (a) $a/h = 5$**, (b)** $a/h = 10$**, (c)** $a/h = 50$ **and (d)** $a/h = 100$**.**

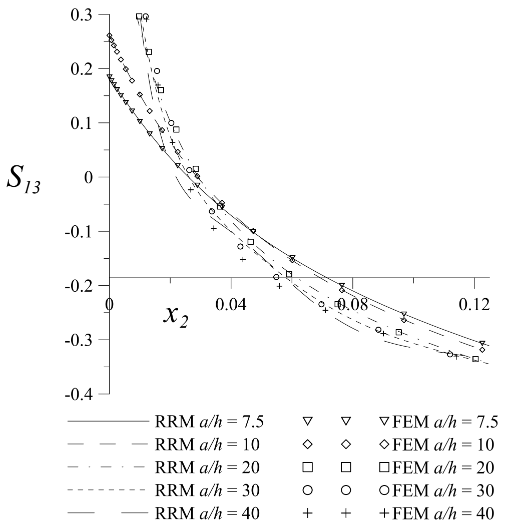

(a)

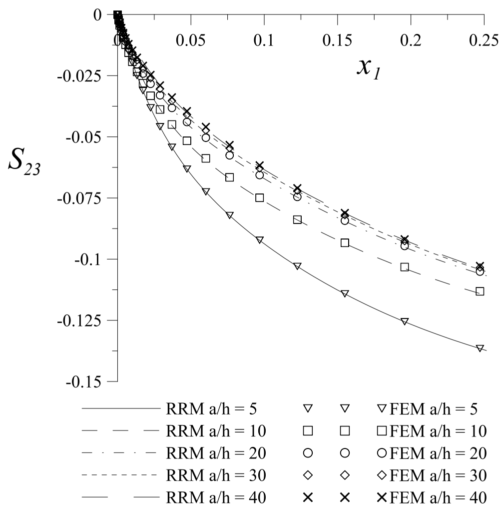

(b)

Figure 8: Comparison between *pb-2* RRM and FEM results of transverse shear in boundary edge for (a) SSSS and (b) HHHH square plates

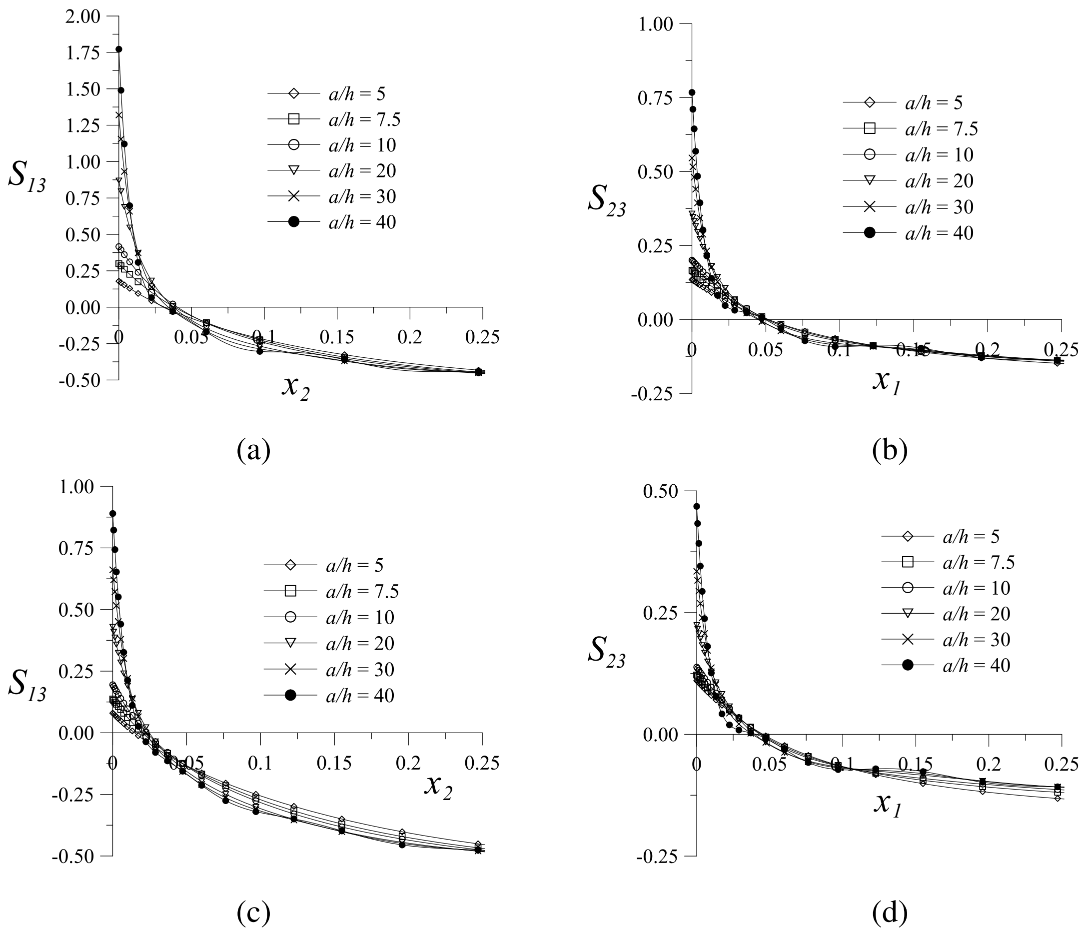

Figure 9: S_{13} **and** S_{23} **of SSSS square plates for** α **equal to (a) 10, (b) 20, (c) 30 and (d) 40.**

center this influence is almost null.

If one studies the effect of different boundary conditions at the corner, interesting results are derived. For SHSH plates, for example, S_{23} response, at the soft-simply supported edge resembles its respective in the hard boundary condition. The opposite correspondence is observed in S_{13}, at the hard simply-supported edge: it simulates the soft boundary condition response. This characteristics is independent from the material properties and the plate's aspect ratio. The differences between the responses of both S_{13} (away from the corner) and S_{23} appear to small in smaller α. The twisting moment M_{12} is null at the corner, growing quickly however, as it goes away from the corner. Moreover, as α increases, differences in the form and in the magnitude between the responses for the a/h assessed tend to become greater.

Conclusions

The *pb-2* Rayleigh-Ritz method is applied to approximate the solution space of thick plates in order to assess two interesting behaviours: anticlastic curvature and transverse shear close to non-smooth regions. Firstly, the thick plate's governing equations were presented and applied to RRM and then the solution procedure was assembled and its convergence was shown.

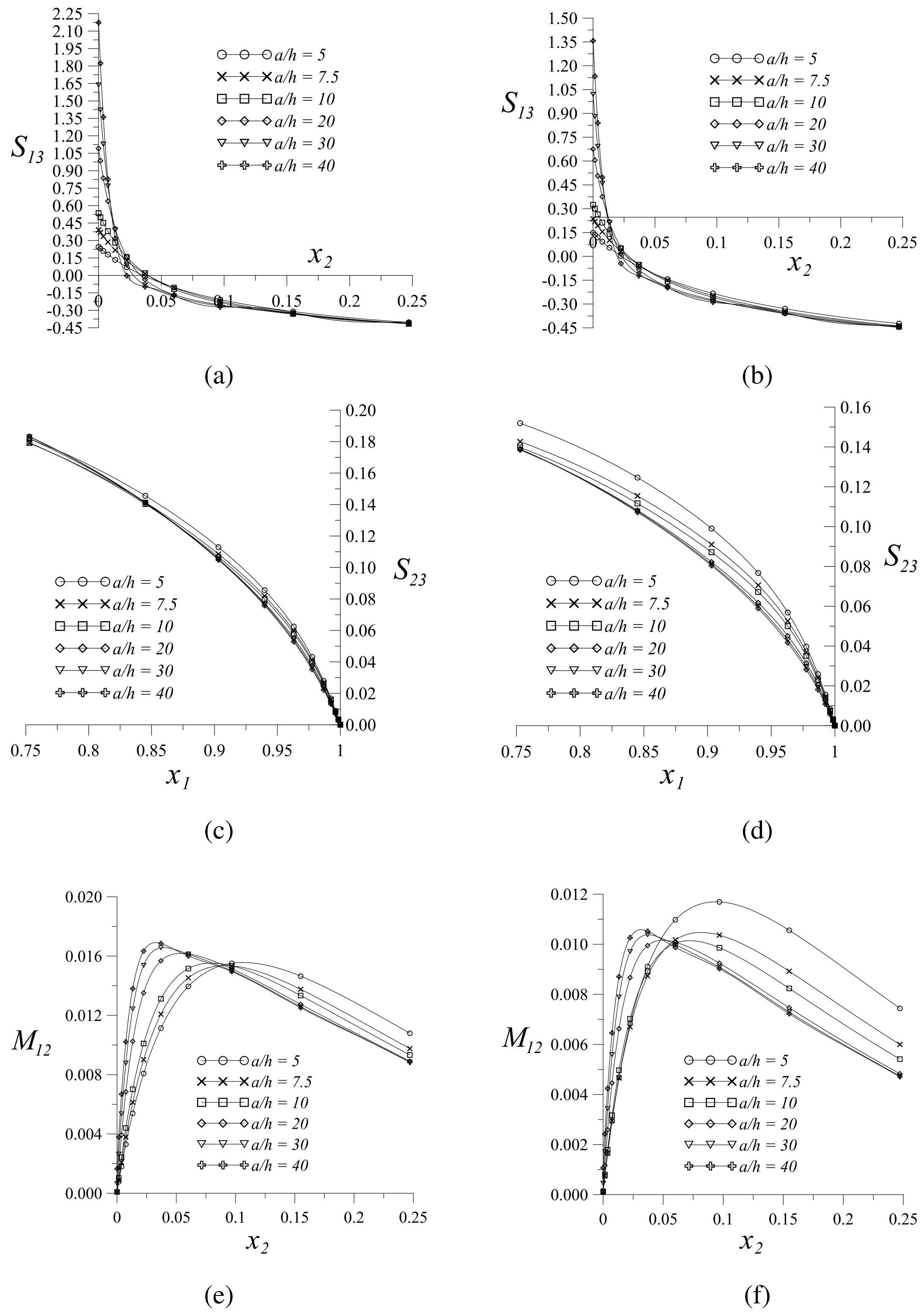

Figure 10: Transverse Shear close to the south-east corner in SHSH square plates with (a) S_{13} **for** $\alpha = 10$ **and** $x_1 = 1$**, (b)** S_{13} **for** $\alpha = 20$ **and** $x_1 = 1$**, (c)** S_{23} **for** $\alpha = 10$ **and** $x_2 = 0$**, (d)** S_{23} **for** $\alpha = 20$ **and** $x_2 = 0$**, (e)** M_{12} **for** $\alpha = 10$ **and** $x_1 = 1$ **and, (f)** M_{12} **for** $\alpha = 20$ **and** $x_1 = 1$

Three cases of anticlastic curvature were presented where it was evaluated its correlation with thickness, degree of anisotropic (via α) and boundary conditions. As aforementioned, the Poisson's ratio greatly influences this effect. An interesting case is presented, in which the minor curvature changes its direction as it gets closer to the free edge.

The study on the transverse shear at corners was also presented and the same parameters were varied so as to verify the sensibility of such parameters to the transverse shear response. Is was verified that, at the corners, both α and a/h may greatly affect the magnitude. Both influence tend to diminish as the evaluation region gets closer to the edge's center.

ACKNOWLEDGEMENTS

Marczak and Lisbôa would like to acknowledge CAPES (Coordination for the Improvement of Higher Educational Personnel) and CNPq (National Council for Scientific and Technological Development) for funding the research project.

REFERENCES

Alternbach, H. (1998). Theories for laminated and sandwich plates. *Mechanics of Composite Materials*, *34*(3), 243–252. doi: 10.1007/BF02256043

Ansys ® Inc. (2017). *User guide*. Author

Bhat, R. B. (1985). Plate deflections using orthogonal polynomials. *Journal of Engineering Mechanics*, *111*(11), 1301–1309. doi: 10.1061/(ASCE)0733-9399(1985)111:11(1301)

Chadwick, P., Vianello, M., & Cowin, S. C. (2001). A new proof that the number of linear elastic symmetries is eight. *Journal of the Mechanics and Physics of Solids*, *49*(11), 2471–2492. doi: 10.1016/S0022-5096(01)00064-3

Cowin, S. C., & Mehrabadi, M. M. (1995). Anisotropic symmetries of linear elasticity. *Applied Mechanics Reviews*, *48*(5), 247–285. doi: 10.1115/1.3005102

Haggblad, B., & Bathe, K.-J. (1990). Specifications of boundary conditions for reissner/mindlin plate bending finite elements. *International Journal for Numerical Method in Engineering*, *30*(5), 9981–1011.

Hanna, N. F., & Leissa, A. W. (1994). A higher order shear deformation theory for the vibration of thick plates. *Journal of Sound and Vibration*, *170*(4), 545–55X.

Hyer, M. W., & Bhavani, P. C. (1984). Suppression of anticlastic curvature in isotropic and composite plates. *International Journal of Solids and Structures*, *20*(6), 553–570.

Jemielita, G. (2002). Symmetry classes for elasticity tensors. *Journal of Theoretical and Applied Mechanics*, *40*(1), 73–84.

Kitipornchai, S., Xiang, Y., Liew, K. M., & Lim, M. K. (1994). A global approach for vibration of thick trapezoidal plates. *Computers & Structures*, *53*(1), 83–92. doi: 10.1016/0045-7949(94)90132-5

Liew, K. M. (1992). Response of plates of arbitrary shape subject to static loading. *Journal of Engineering Mechanics*, *118*(9), 1783–1794. doi: 10.1061/(ASCE)0733-9399(1992)118:9(1783)

Liew, K. M., & Wang, C. M. (1993). *Pb-2* rayleigh-ritz method for general plate analysis. *Engineering Structures*, *15*(1), 55–60. doi: 10.1016/0141-0296(93)90017-X

Liew, K. M., Xiang, Y., & Kitipornchai, S. (1993). Transverse vibration of thick rectangular plates-i. comprehensive sets of boundary conditions. *Computers & Structures*, *49*(6), 1–29. doi: 10.1016/0045-7949(93)90122-T

Lisbôa, T. V., Geiger, F. P., & Marczak, R. J. (2017). A recursive methodology to determine the mechanical response of thin laminated plates in bending (accepted for publication). *Journal of Aerospace Technology and Management*, *9*(4).

Lisbôa, T. V., & Marczak, R. J. (2017). A recursive methodology for the solution of semi-analytical rectangular anisotropic thin plates in linear bending. *Applied Mathematical Modelling*, *48*, 711-730. doi: 10.1016/j.apm.2017.04.020

Lo, K. H., Christensen, R. M., & Wu, E. M. (1977). A high-order theory of plate deformation. *Journal of Applied Mechanics*, *44*(4), 663–668. doi: 10.1115/1.3424154

Mindlin, R. D. (1951). Influence of rotary inertia and shear on flexural motions of elastic plates. *Journal of Applied Mechanics*, *18*, 31–38.

Reddy, J. N. (2004). *Mechanics of laminated composite plates and shells*. Boca Raton: CRC Press.

Reddy, J. N. (2007). *Theory and analysis of elastic plates and shells*. Boca Raton: CRC Press.

Ting, H.-T., & Kim, S.-E. (2012). Analytical solution of a two variable refined plate theory for bending analysis of orthorhombic levy-type plates. *International Journal of Mechanical Sciences*, *54*(1), 269–276. doi: 10.1016/j.ijmecsci.2011.11.007

Ting, T. C. T. (2003). Generalized cowin-mehrabadi theorems and a direct proof that the number of linear elastic symmetries is eight. *International Journal of Solids and Structures*, *40*(25), 7129–7142. doi: 10.1016/S0020-7683(03)00358-5